Enhancing Polysulfide Redox Kinetics Through Synergistic Polarization of Ferroelectric (Ba0.9Sr0.1TiO3) Nanoparticles for High-Capacity Li-S Batteries.

Ivan Castillo *, Balram Tripathi , Danilo Barrionuevo , Karuna K. Mishra , Gerardo Morell , Ram S. Katiyar *

Posted Date: 9 August 2024

doi: 10.20944/preprints202408.0648.v1

Keywords: Li-S battery; C/S composite; BST coupling; polysulfide trapping; ferroelectric material

Article

Enhancing Polysulfide Redox Kinetics through Synergistic Polarization of Ferroelectric ($Ba_{0.9}Sr_{0.1}TiO_3$) Nanoparticles for High-Capacity Li-S Batteries

Ivan Castillo [1,2,3,*], Balram Tripathi [1], Danilo Barrionuevo [2], Karuna K. Mishra [1], Gerardo Morell [1] and Ram S. Katiyar [1,*]

[1] Department of Physics and Institute for Functional Nanomaterials, P.O. Box 70377, San Juan, PR-00936-8377, USA
[2] Department of Mathematics and Physics, University of Puerto Rico, Cayey, PR 00736, USA
[3] Deparment of Science and Technology, Ana G. Mendez University, Cupey, PR 00926, USA
* Correspondence: ivanwalter.castillo@upr.edu (I.C.); ram.katiyar@upr.edu (R.S.K.)

Abstract: We report on the role of synergistic polarization of $Ba_{0.9}Sr_{0.1}TiO_3$ (BST) nanoparticles in sulfur cathodes to enhance the redox kinetics of polysulfides for high-capacity Li-S batteries. Ferroelectric nanoparticles are known to significantly improve the electrochemical performance of Li-S batteries due to their inherent self-polarization and high adsorption capacity towards polysulfides. X-ray diffraction spectra confirmed the tetragonal symmetry (c/a=1.0073), while Raman spectroscopic analysis validated the presence of tetragonal orientation Raman modes in BST-modified composites. Scanning electron microscope (SEM) images showed a homogeneous distribution of BST in the sulfur cathode system, with grain sizes ranging from 1 to 1.5 μm. Notably, the BST-coupled $S_{50}BST_{30}CB_{10}PVDF_{10}$ composite cathode achieved a capacity of approximately 820 mAh/g at 100 mA/g, maintaining stability over 100 cycles, demonstrating improved electrochemical performance. Two distinct plateaus between 2.3 V to 2.0 V and 2.0 V to 1.5 V further underscore the superior performance of BST ferroelectric nanoparticles in enhancing the redox kinetics of Li-S batteries. By leveraging the favourable affinity of polar substances towards polysulfides, we aimed to create a more stable reactive environment within the cathodic site, effectively trapping polysulfide intermediates through the synergistic polarization of BST nanoparticles. The synergistic polarization induced by the asymmetric crystal structure of ferroelectrics is anticipated to generate internal electric fields, enhancing chemisorption with heteropolar reactive. The observed high cyclic stability further validates the efficacy of these composite cathodes in mitigating the polysulfide shuttle effect, offering promising prospects for advancing Li-S battery technology.

Keywords: Li-S battery; C/S composite; BST coupling; polysulfide trapping; ferroelectric material

1. Introduction

Lithium-sulfur (Li-S) batteries represent a promising frontier in energy storage technology, owing to their high energy density and cost-effectiveness [1]. Typically, these batteries comprise cathodes made of elemental sulfur (S_8) and anodes composed of lithium. Leveraging a multi-electron conversion mechanism between S_8 and lithium metals, Li-S batteries offer theoretical specific capacities of 1675 mAh/g and specific energies of 2600 Wh/kg, nearly four times that of conventional Li-ion batteries [2,3]. The working mechanism of Li-S batteries is generally the same as that of lithium-ion batteries, but the difference is that the high capacity and recharge ability of Li-S batteries compared to traditional lithium batteries mainly come from the breaking and formation of S-S bonds. However, the practical application of Li-S batteries faces significant challenges. Firstly, sulfur and

 doi:10.20944/preprints202408.0648.v1

discharge products such as Li_2S_2 and/or Li_2S exhibit low electrical conductivity, hampering battery reaction rates [4,5]. Additionally, insoluble compounds like Li_2S are generated during cycling, covering active compounds, and hindering lithium-ion access while degrading conductive networks. Furthermore, soluble polysulfides of high order can migrate through separators to the lithium negative electrode, where they are reduced to insoluble forms. The diffusion of the soluble polysulfide species from the cathode to the lithium-metal anode results in continuous capacity-loss, parasitic self-discharge, and reduced charge efficiency. These polysulfides further react with fully reduced sulphide's, leading to the concentration of lower-order polysulfides at the anode side, which diffuse back to the positive electrode and undergo re-oxidation, perpetuating a shuttle effect [4–6]. This shuttle induces the deposition of solid Li_2S_2 and Li_2S on the anode, resulting in low Columbic efficiency, reduced utilization of sulfur cathodes, and severe degradation of cycle life. To address these issues, extensive efforts have focused on enhancing cathode electrical conductivity and suppressing the loss of soluble polysulfide intermediates during cycling. Composite cathodes incorporating conductive nanocarbons (e.g., mesoporous carbon, carbon nanotubes, graphene, carbon hollow spheres) as well as polymers like polyaniline and polyacrylonitrile have demonstrated enhanced conductivity, robust electron/ion pathways, and superior charge-discharge capacity and cycling performance [7,8,17–20,9–16]. Effectively retarding polysulfide shuttle remains crucial for achieving Li-S cells with superior storage performance. One promising strategy involves constructing functional porous and conductive hosts to immobilize sulfur and anchor lithium polysulfides [16]. Recent studies have highlighted the effectiveness of ferroelectric materials in mitigating polysulfide shuttle. For instance, Wei et al. demonstrated that ferroelectric barium titanate ($BaTiO_3$) effectively anchors polysulfides via built-in electric fields arising from spontaneous polarization, leading to significantly improved electrochemical performance [21]. Similarly, reports have showcased the role of spontaneously polarized bismuth ferrite ($BiFeO_3$) in suppressing polysulfide shuttle in Li-S batteries [22]. (Ba, Sr) TiO_3 has garnered significant attention due to its strong dielectric and ferroelectric polarization properties under electric fields. By introducing strontium (Sr) into $BaTiO_3$, researchers have achieved high dielectric constants and low leakage currents [23,24]. Additionally, in the nanoscale regime, the ferroelectric structure exhibits distinct characteristics from bulk materials, with grain size playing a crucial role in determining electrical properties [25]. In this manuscript, we present the suppression of polysulfides shuttle via $Ba_{0.9}Sr_{0.1}TiO_3$, a highly polarized ferroelectric additive in sulfur/carbon black composite cathodes, aiming to enhance the energy density of Li-S batteries.

2. Experimental:

2.1. Materials & method

Sulfur (S, purity 99.5%), Carbon black (99.00%), N-Methyl 1-2-pyrrolidone (NMP 98%) were purchased from Sigma Aldrich and used without further purification. $Ba_{0.9}Sr_{0.1}TiO_3$ (BST) where in BST_x (x = 0.2 & 0.3) samples were prepared by high-energy ball milling and solid-state reaction method. The stoichiometric ratio of starting raw materials $BaCO_3$ (99.997%), $SrCO_3$ (99.998%), and TiO_2 (99.988%) were mixed along with isopropanol using planetary ball milling (Pulverisette Fritsch Planetary Mill). The powder was screened using a mesh of 150 μm size to obtain a fine powder of almost uniform particle size. The powder was pre-calcined at 850°C/4 h, followed by thorough pulverization and calcined at 1150°C/2 h at a ramp rate of 5°C/min. The ball milling was suspended for 20 min after every 1 h of milling to cool down the milling system. The aluminium (Al) foil (25μm thickness and purity 99.45%), Lithium foil, (0.75×19mm, 99.9%) and polypropylene separator (Celgard®2400:25 μm), Bis(trifluoromethylsulfonyl)imide lithium salt (LiTFSI; 98+%), lithium nitrate ($LiNO_3$; anhydrous, 99.999%), 1,2-dimethoxyethane (DME; 99+%), 1,3-dioxolane (DOL; 99.5%) were purchased from Alfa Aesar and used without further purification for the preparation of 1M LiTFSI as the electrolyte. The sulfur (S), BST, carbon black (CB) and PVDF were mixed. The slurry of S/BST/CB/PVDF composite was prepared in NMP via ball milling and coated on aluminium foil of thickness (25μm) via doctor blade. After drying in vacuum oven (40°C) till 15 hrs. electrodes were

 doi:10.20944/preprints202408.0648.v1

cut into disc of 13 mm for cathode. The polypropylene (PP) separator (Celgard 2400) was used. The coin cells (CR2032) were assembled in an Ar-filled glove box (MBraun, USA) with H_2O, and O_2 <0.1ppm.

2.2. Characterization

The X-ray diffraction (XRD) measurements were carried out using a Rigaku Smart Lab X-ray diffractometer equipped with CuK_α radiation (λ = 1.5418 Å) operated in a Bragg-Brentano (θ–2θ) geometry at 40 kV and 44 mA. The crystal structure and phase purity of the compounds were checked in a slow scan mode using a 2θ step size of 0.05°. The analyses of the XRD patterns were carried out using FullProf suite software 7.70 (Version April 2022). Raman spectroscopy studies were carried out employing a HORIBA Jobin Yvon micro-Raman spectrometer (model: T64000) equipped with a 50× long working distance objective lens in a back-scattering geometry (2θ = 180°) using a 514.5 nm line of an Ar^+ ion laser (Coherent, Innova 70-C). Raman spectra with improved signal-to-noise ratio were measured by optimizing the laser power and acquisition time.

The surface morphology of the samples was studied using scanning electron microscopy (SEM) (model: JEOL/MP) equipped with a backscattered electron detector operating at an accelerating voltage of 20 kV and 3300× magnifications. SEM-based energy dispersive X-ray spectra (EDS) (model: JSM-IT500HR-JEOL) were measured from the crack surface of the sintered pellets to infer their chemical compositions. Galvanostatic charge-discharge curves were measured using MTI battery tester at different current densities within the voltage range 1.5-3.2 V (Vs Li^+/Li). The cyclic voltammetry @ 0.1mV/s was used for the testing of cycling performance and stability of the cathode material. Electrochemical impedance spectroscopy (EIS) was performed on symmetric cells of $S_{60}BST_{20}CB_{10}PVDF_{10}$ & $S_{50}BST_{30}CB_{10}PVDF_{10}$ using an Arbin-32MTS Pro battery tester at open circuit potential (OCP) with a signal amplitude of 10 mV, in a frequency range from 1 MHz to 50 Hz.

3. Results & discussion

3.1. X-ray diffraction

Figure 1 represents X-ray diffraction spectra of pristine carbon black, $Ba_{0.9}Sr_{0.1}TiO_3$ (x = 0.1), Carbon black, Sulfur, $S_{50}BST_{30}C_{10}PVDF_{10,}$ & $S_{60}BST_{20}C_{10}PVDF_{10}$ composites obtained from Rietveld analysis of the high-resolution powder XRD patterns measured in the angle (2θ) range from 10º to 100º at room temperature. The $S_{60}BST_{20}CB_{10}PVDF_{10}$ & $S_{50}BST_{30}CB_{10}PVDF_{10}$ composite cathode material shows all the sulfur diffraction peaks, together with an extra peak at 25.60º, showing the carbon (002) diffraction peak together with BST diffraction peaks, consistent with ICDD # 861518. However, variation in the intensity of peaks indicates the lack of long-range order due to sulfur confinement into carbon and BST. The size of sulfur particles is ~20–25 nm, and that of carbon is 30–40 nm, as estimated from the Scherrer formula [26,27].

 doi:10.20944/preprints202408.0648.v1

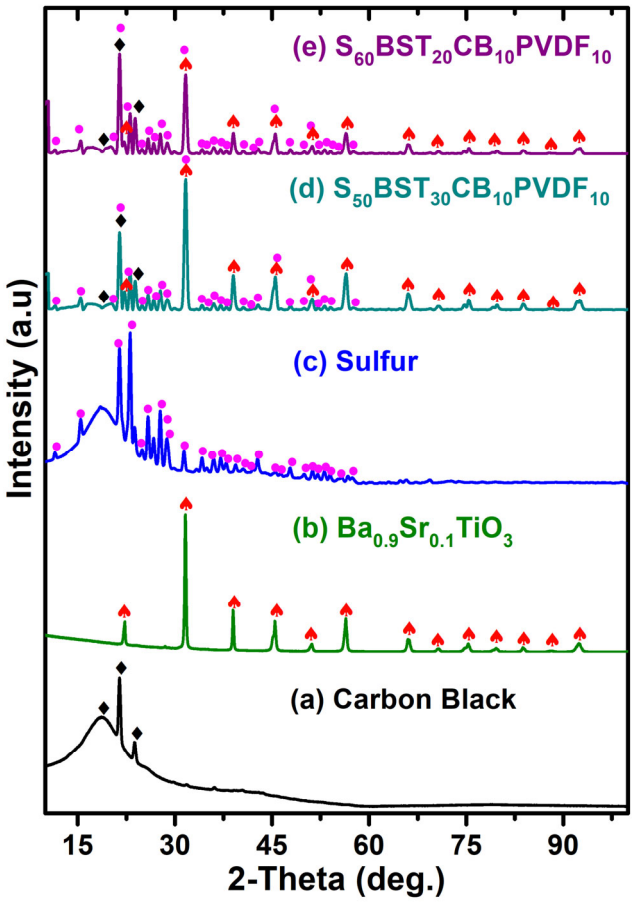

Figure 1. X-ray diffraction spectra for (a) Carbon black (b) BST (c) Sulfur (d) $S_{50}BST_{30}C_{10}PVDF_{10}$ (e) $S_{60}BST_{20}C_{10}PVDF_{10}$.

3.2. Raman spectra

Figure 2(a, b, c, d, e, f) show Raman spectra of pristine $Ba_{0.9}Sr_{0.1}TiO_3$, carbon black, sulfur, $S_{60}BST_{20}C_{10}PVDF_{10}$, $S_{50}BST_{30}CB_{10}PVDF_{10}$ composites & polarization loop(p-E) of $Ba_{0.9}Sr_{0.1}TiO_3$ respectively. Raman spectroscopic study confirms Raman modes ($A_1(TO_1)$, $A_1(TO_2)$, $A_1(TO_3)$ and $A_1(LO_3)$) of the tetragonal orientation for BST modified composites. The low wavenumber peaks noticed in Figure 2(e) at 26, 44, 49, and 84, correspond to A1(LO) phonon modes, whereas vibrational peaks noticed at 153, 217, and 471 cm^{-1} correspond to E(TO) modes for the BST system. The observation of these modes substantiates the phase purity of BST nanoparticle's tetragonal structure [28]. The characteristic carbon peaks are identified at 1350 and 1580 cm^{-1}, which correspond to D and G characteristic bands [29]. These characteristic carbon vibration modes are observed in all S/BST/CB/PVDF composite samples. Figure 2 (c, d), suggesting the efficient integration of carbon into the S/BST/CB/PVDF composite matrix. Further, the rhombic sulfur characteristics are observed in all S/BST/CB/PVDF composite cathode materials, implying the efficient impregnation of sulfur with carbon in these composite cathode samples.

 doi:10.20944/preprints202408.0648.v1

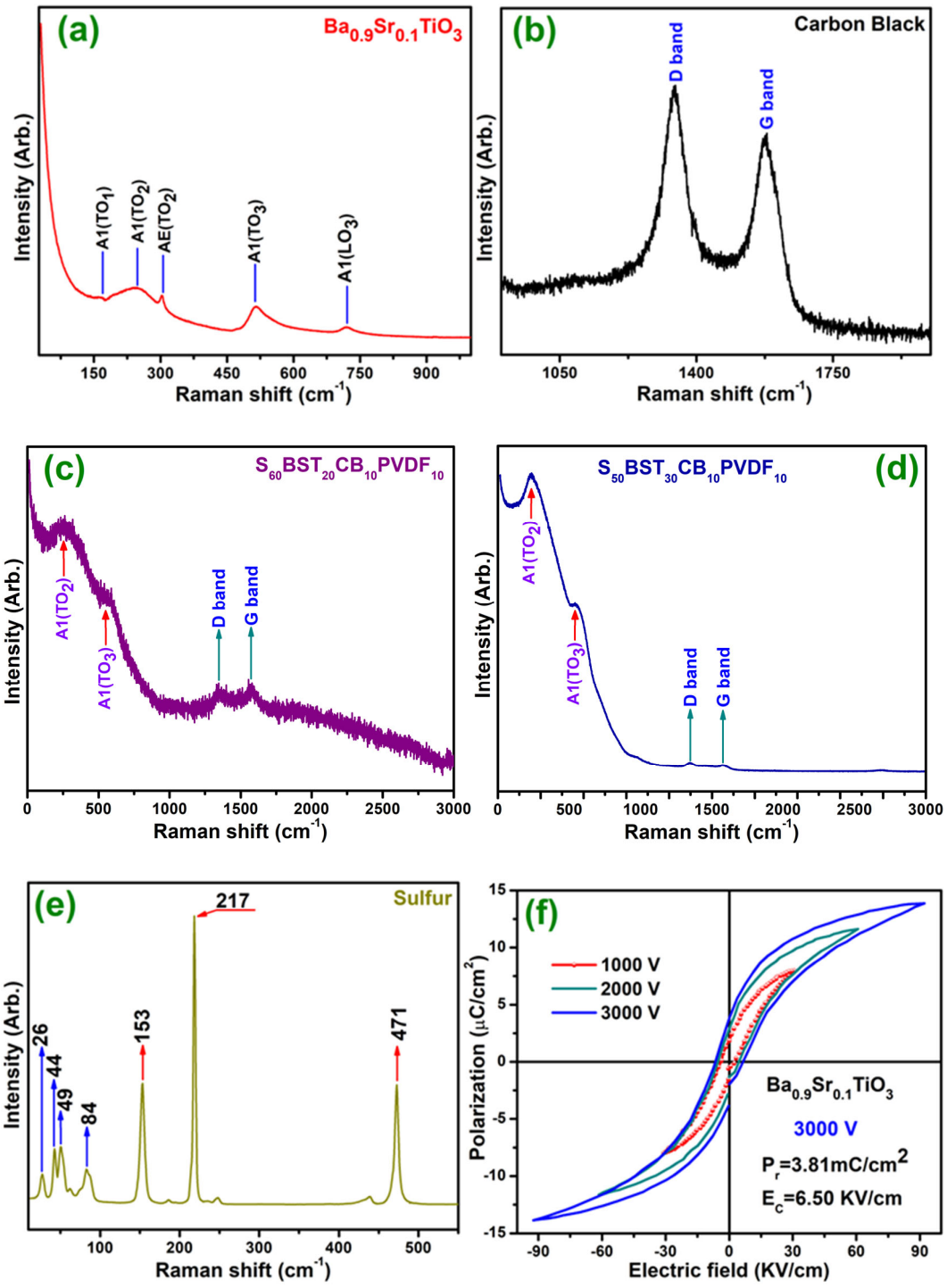

Figure 2. Raman spectra of (a) $Ba_{0.9}Sr_{0.1}TiO_3$ (b) Carbon black, (c) $S_{50}BST_{30}C_{10}PVDF_{10}$, (d) $S_{60}BST_{20}CB_{10}PVDF_{10}$ composites, (e) Sulfur & (f) Polarization loop(P-E) of $Ba_{0.9}Sr_{0.1}TiO_3$.

As shown in Figure 2(f) the BST ferroelectric particles, contributing the polarization which induces modifications in S/CB/PVDF composite cathode. Generally, polar substances have an affinity toward polysulfides and can provide more stable reacting environment at the cathode site [21,30]. It is well known that the ferroelectric materials induce permanent dielectric polarizability via which suppression of polysulfide intermediates is expected. This force is determined to alter the path of

 doi:10.20944/preprints202408.0648.v1

dissolved charged polysulfide ions, thus enhancing electrochemical performance by promoting the suppression of these polysulfide ions.

3.3. Surface morphology

Figure 3 (a, b) shows SEM images of $S_{60}BST_{20}C_{10}PVDF_{10}$, $S_{50}BST_{30}CB_{10}PVDF_{10}$, and Figure 3(c, d) shows EDAX spectra of $S_{60}BST_{20}C_{10}PVDF_{10}$ & $S_{50}BST_{30}CB_{10}PVDF_{10}$ composites. The material surrounding to sulfur matrix as observed is acting as a protective layer, showing the morphology of $S_{60}BST_{20}CB_{10}PVDF_{10}$, & $S_{50}BST_{30}CB_{10}PVDF_{10}$ composite materials. The surface area and structural features provides defect sites at which lithium ions may be adsorbed to the surface of loosely bound carbon layers [31]. This network structure showing the close contact between BST, CB, and sulfur, may be an excellent electron pathway for insulating sulfur and adsorption sites for soluble polysulfides.

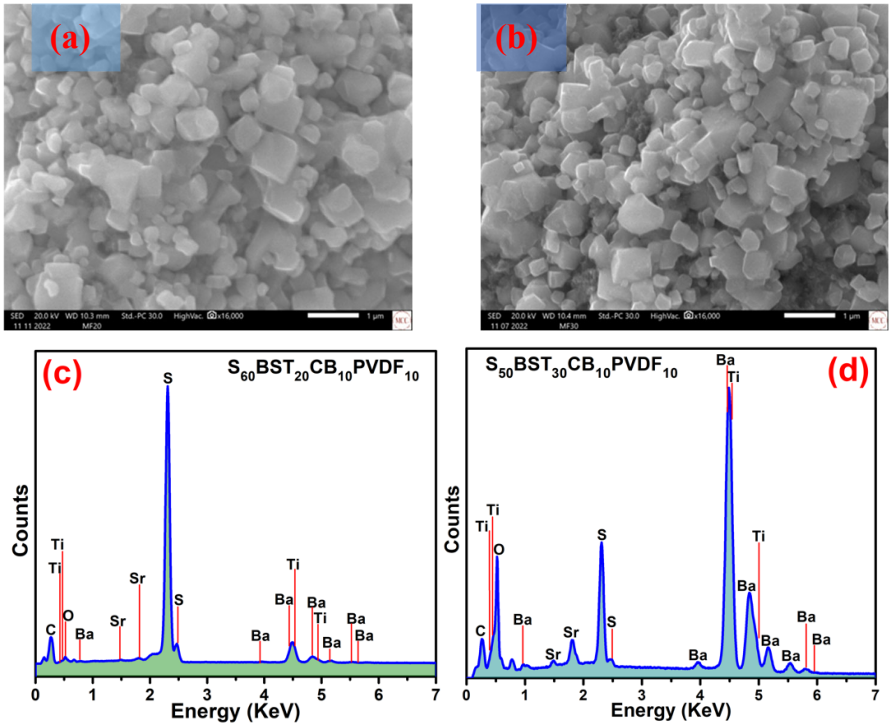

Figure 3. SEM images of (a)$S_{60}BST_{20}CB_{10}PVDF_{10}$ (b) $S_{50}BST_{30}CB_{10}PVDF_{10}$ EDAX spectra of (c) $S_{60}BST_{20}CB_{10}PVDF_{10}$ (d) $S_{50}BST_{30}CB_{10}PVDF_{10}$ composites.

3.5. Electrochemical performance

3.5.1. Charge-discharge

Figure 4(a, c, e, g) showing charge-discharge profiles for $S_{60}BST_{20}CB_{10}PVDF_{10}$, and $S_{50}BST_{30}CB_{10}PVDF_{10}$ @100mA/g & 200mA/g respectively up to 100 cycles. As shown in fig 4 (a, c) it has been observed that the maximum capacity for $S_{60}BST_{20}CB_{10}PVDF_{10}$ composite cathode @ 100 mA/g in 1st cycle is 750 mAh/g which reduces to 348 mAh/g after 100th cycle with capacity retention of 46.4%. However, the observed specific capacity of the same composite cathode of $S_{60}BST_{20}CB_{10}PVDF_{10}$ @ 200 mA/g in 1st cycle is 300 mAh/g which reduces to 246 mAh/g after 100th cycle. In this study, LITFSI electrolyte with $LiNO_3$ was used with amount of 12 $\mu L mg^{-1}$ had a high CE of 95%, indicating that the poly-shuttle effect was limited. However, a low-capacity retention after 100 cycles and capacity fade along the cycling process was observed. While in case of BST coupled cathode capacity fade has been found to be reduced due to build in electric field due to polarization nature of BST which provides electrostatic repulsion to retard the polysulfides and improves the capacity.

 doi:10.20944/preprints202408.0648.v1

The specific capacity for $S_{50}BST_{30}CB_{10}PVDF_{10}$ @100mA/g in 1st cycle is 820 mAh/g which reduces to 400 mAh/g after 100th cycle with capacity retention of 48.7%, However the observed specific capacity of $S_{50}BST_{30}CB_{10}PVDF_{10}$ composite cathode @ 200 mA/g in 1st cycle is 565 mAh/g which reduces to 311 mAh/g after 100th cycle with capacity retention 55%. The enhanced capacity retention observed in the $S_{50}BST_{30}CB_{10}PVDF_{10}$ composite cathode, attributed to the higher concentration of BST, reaches up to 59.6%. The lower voltage plateaus in the initial cycle indicated high polarization of the sulfur cathode during the reaction time. After the initial cycle, most of the active sulfur materials dissolved into the liquid electrolyte and rearranged in the cathode, thus showing an increase in the discharge plateaus. Sulfur composites could realize solid-state transformation due to the strong interactions between sulfur and BST matrix, which is beneficial to completely inhibit shuttle effect and enable compatibility with carbonate-based electrolytes. Therefore, the exploration of more indigenous design of cathode and combination with other strategies should be considered. In addition, it is found that BST intercalated sulfur cathode greatly enhanced the capacities and decreased the voltage difference between charge and discharge plateaus. This improvement suggests that the spontaneous ferroelectric polarization of BST nanoparticles facilitates the migration of Li-ions and mitigates the concentration gradient of Li-ions near the electrode surface, thereby controlling polysulfide formation [32]. The coupling of BST nanoparticles effectively anchors polysulfides in the cathode. With the addition of spontaneously polarized BST particles, dissoluble heteropolar polysulfides are likely absorbed around the nanoparticles due to induced internal electric fields. This attribute controlled reactions from S_8 to Li_2S_2 or Li_2S_4. Moreover, the strong polarization of ferroelectric nanoparticles influences the distribution of Li-ions, creating diffusion pathways within the electrolyte/active material.

 doi:10.20944/preprints202408.0648.v1

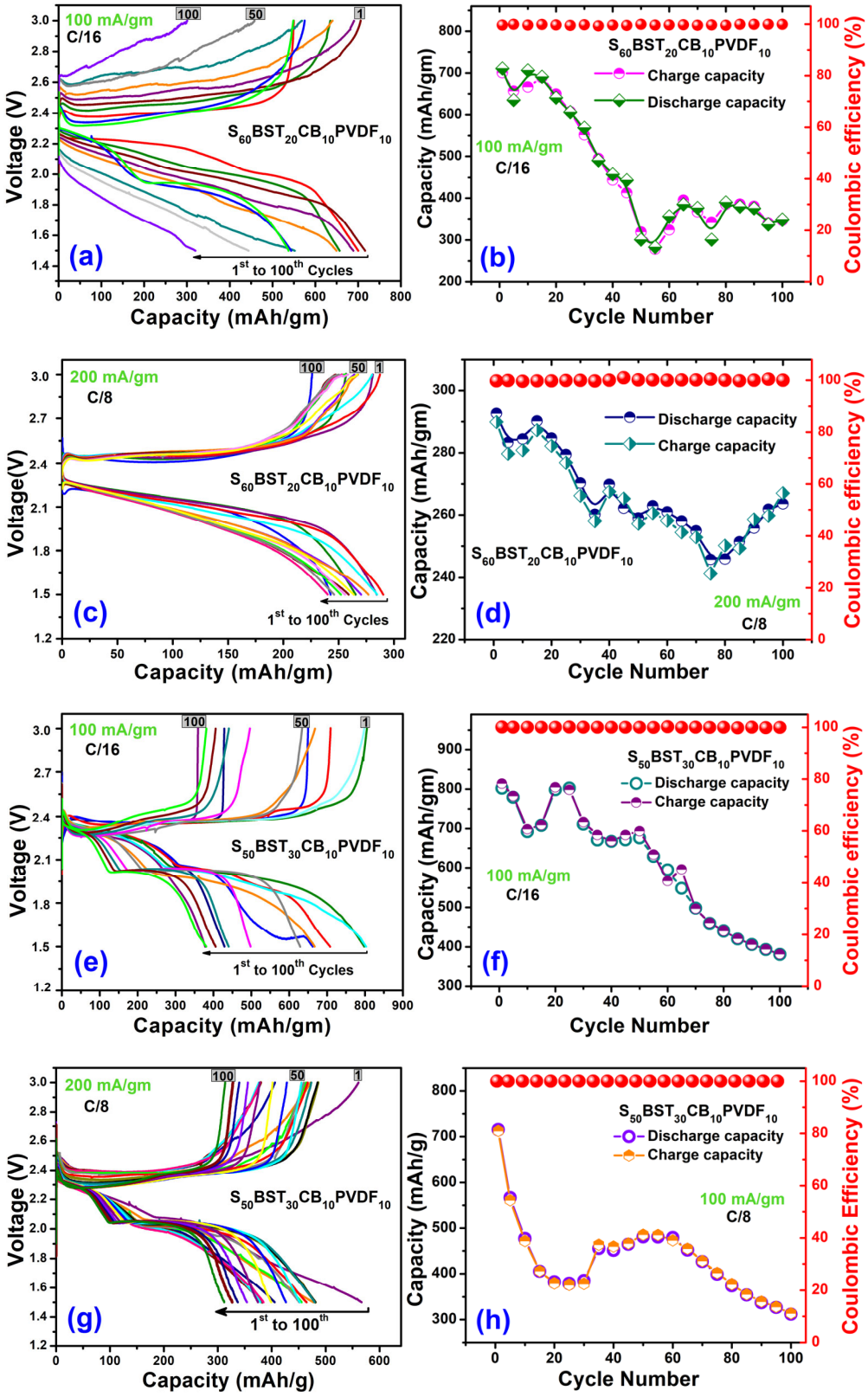

Figure 4. Capacity vs voltage performance of $S_{60}BST_{20}CB_{10}PVDF_{10}$ (a)100mA/g & (c) 200mA/g, $S_{50}BST_{30}CB_{10}PVDF_{10}$ (e)100 mA/g & (g)200 mA/g, Cycling performance of $S_{60}BST_{20}CB_{10}PVDF_{10}$ (b)100 mA/g & (d) 200 mA/g, $S_{50}BST_{30}CB_{10}PVDF_{10}$ (f) 100 mA/g & (h) 200 mA/g.

 doi:10.20944/preprints202408.0648.v1

This accelerates the transfer speed of Li-ions, potentially eliminating the concentration gradient near the deposition surface. Consequently, the internal electric field of ferroelectric BST particles plays a crucial role in inhibiting LiPSs shuttling, thereby improving the cycle stability of Li-S batteries. The observed capacity retention (CR%) has been significantly enhanced for S/BST/CB/PVDF composite cathodes @ 100 mA/g.

3.5.2. Cyclic voltammetry & EIS performance

Figure 5 (a, c) presents the cyclic voltammetry (CV) curves for S/BST/CB/PVDF composite cathodes @0.1 mV/s. The diffusion of Li^+ could be accelerated through designing structure and doping modifications that further promote the electrochemical kinetics of sulfur. Typically, in Li-S battery cathode materials, two reduction peaks are observed during cycling. The higher peak corresponds to the transformation of elemental sulfur (S_8) into long-chain polysulfides (Li_2S_n, n>4), while the lower peak corresponds to the conversion of long-chain polysulfides into short-chain polysulfides (Li_2S_n, n< 4) and the final product of lithium sulfide (Li_2S) [33]. The CV analysis of the $S_{60}BST_{20}CB_{10}PVDF_{10}$ composite cathode shows oxidation peaks at 2.7 V and 2.5 V, with a reduction peak at 2.0 V during cycling. In contrast, the $S_{50}BST_{30}CB_{10}PVDF_{10}$ composite exhibits oxidation peaks at 2.6 V and 2.7 V and reduction peaks at 2.0 V and 2.2 V. This shift in peak positions indicates enhanced reduction kinetics due to the incorporation of BST nanoparticles. The improved kinetics may be attributed to the coupling of ferroelectric nanoparticles, facilitating the reversible transformation of Li_2S to short and long-chain LiPSs, and ultimately to S_8[21]. Figure 5 (b, d) displays the EIS spectra of the $S_{60}BST_{20}CB_{10}PVDF_{10}$ and $S_{50}BST_{30}CB_{10}PVDF_{10}$ composite cathodes. Symmetric cells with positive and blocking electrodes confirm that sulfur, as the active material, does not contribute to the resistance of the positive electrode. The inclusion of BST at 20 and 30 wt.% and the application of the RC(R)W circuit model for interfacial parameters yielded the following values for $S_{60}BST_{20}CB_{10}PVDF_{10}$: R_s (1.142 Ω), C (1.333 μF), R_{ct} (289.5 Ω), and W (0.003719). For $S_{50}BST_{30}CB_{10}PVDF_{10}$, the observed values were R_s (2.688 Ω), C (9.1 μF), R_{ct} (145 Ω), and W (0.02312). These results indicate improved lithium-ion diffusion pathways [34]. BST stands out as a unique and promising catalyst due to the significant effects of polarization on its surface. The built-in electric field within ferroelectric materials promotes atomic reconstruction, facilitating the adsorption or desorption of certain atoms on the material's surface. Additionally, the differing electrostatic potential and electron distribution of ferroelectric materials lead to varied surface chemical activity and redox reaction capabilities [35]. This characteristic of BST enhances the redox kinetics in the Li-S battery, contributing to the overall improved electrochemical performance observed in the composite cathodes. The ferroelectric nature of BST not only aids in polysulfide trapping through synergistic polarization but also enhances the chemisorption of reactive species, ultimately mitigating the polysulfide shuttle effect and advancing the development of high-capacity, stable Li-S batteries.

 doi:10.20944/preprints202408.0648.v1

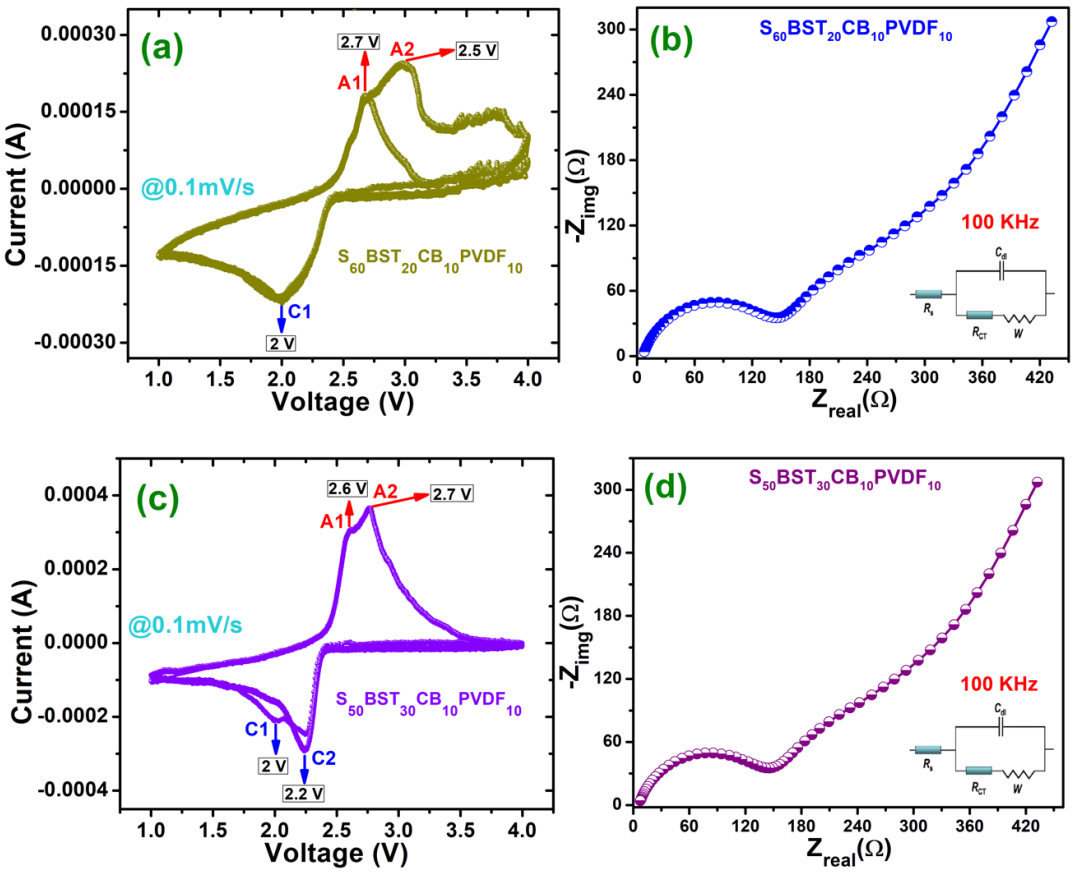

Figure 5. (a, c) Cyclic voltammogram & EIS spectra of $S_{60}BST_{20}CB_{10}PVDF_{10}$ (b, d) Cyclic voltammogram & EIS spectra of $S_{50}BST_{30}CB_{10}PVDF_{10}$ composite electrodes.

4. Conclusions

In summary, polycrystalline BST_x (x = 0.2 & 0.3) ferroelectric nanoparticles were successfully intercalated into S/CB composite cathodes using a combination of high energy ball milling and the solid-state reaction method. Rietveld analysis of XRD data confirmed the formation of single-phase compounds, with BST exhibiting a tetragonal phase. Ferroelectric polarization studies indicated a maximal polarization of approximately 14.58 μC/cm² for BST. SEM images revealed an interconnected network of composites on the surface morphology. Li-S batteries constructed with optimized hybrid cathodes, such as $S_{50}BST_{30}CB_{10}PVDF_{10}$ & $S_{60}BST_{20}CB_{10}PVDF_{10}$ composites, and tested at 100 mA/g & 200 mA/g with a polypropylene (PP) separator, exhibited specific capacities of approximately 820 mAh/g & ~540 mAh/g, respectively, along with enhanced capacity retention of up to 60%. This improvement in capacity retention can be attributed to the effective suppression of polysulfides facilitated by the spontaneous polarization provided by the ferroelectric nanoparticles. The BST intercalated sulfur/CB composite host show better performance might be due to the ferroelectric polarization into the host. The composite system, delivers excellent rate performance because of the effective control of polysulfides and additional enhanced Li^+ transport. The presence of BST particles within the cathode likely acts as adsorption centres for polysulfides, thereby minimizing their exposure to the electrolyte. This strategy, involving the induction of ferroelectric polarization within the cathode, offers a promising solution to control polysulfide formation and achieve improved capacity retention in high energy Li-S batteries. As a key direction for future battery development, Li-S batteries are set to find extensive applications across the energy and automotive industries, among others.

 doi:10.20944/preprints202408.0648.v1

Acknowledgements: The authors are grateful for the financial support from NSF- EPSCoR Grant #OIA-1849243 for the Centre for advancement of wearable technologies (CAWT), NASA MIRO PR-SPRInT Grant #80NSSC19M0236, and NASA EPSCoR Grant #80NSSC19M0049.

References

1. Li, Y. & Guo, S. Material design and structure optimization for rechargeable lithium-sulfur batteries. *Matter* 2021, 4, 1142–1188.
2. Hou, L. P., Zhang, X. Q., Li, B. Q. & Zhang, Q. Challenges and promises of lithium metal anode by soluble polysulfides in practical lithium–sulfur batteries. *Materials Today* 2021, 45, 62–76.
3. Yang, Y., Zheng, G. & Cui, Y. Nanostructured sulfur cathodes. *Chemical Society Reviews* 2013, 42, 3018–3032.
4. Su, Y. Challenges and Prospects of Lithium À Sulfur Batteries. 2013, 46, 1125–1134.
5. Ji, X. & Nazar, L. F. Advances in Li-S batteries. *Journal of Materials Chemistry* 2010, 20, 9821–9826.
6. Ji, X., Lee, K. T. & Nazar, L. F. A highly ordered nanostructured carbon-sulphur cathode for lithium-sulphur batteries. *Nature Materials* 2009, 8, 500–506.
7. Xin, S., Yin, Y. X., Wan, L. J. & Guo, Y. G. Encapsulation of sulfur in a hollow porous carbon substrate for superior Li-S batteries with long lifespan. *Particle and Particle Systems Characterization* 2013, 30, 321–325.
8. Li, D. *et al.* High sulfur loading cathodes fabricated using peapodlike, large pore volume mesoporous carbon for lithium-sulfur battery. *ACS Applied Materials and Interfaces* 2013, 5, 2208–2213.
9. Sun, F. *et al.* High efficiency immobilization of sulfur on nitrogen-enriched mesoporous carbons for LI-S batteries. *ACS Applied Materials and Interfaces* 2013, 5, 5630–5638.
10. Zhou, G. *et al.* A flexible nanostructured sulphur-carbon nanotube cathode with high rate performance for Li-S batteries. *Energy and Environmental Science* 2012, 5, 8901–8906.
11. Susanne, D. W. *et al.* High capacity vertical aligned carbon nanotube/sulfur composite cathodes for lithium–sulfur batteries. *Chemical Communications* 2012, 48, 4097–4099.
12. Liu, X. *et al.* Hierarchical nanostructured composite cathode with carbon nanotubes as conductive scaffold for lithium-sulfur batteries. *Journal of Energy Chemistry* 2013, 22, 341–346.
13. Hagen, M. *et al.* Lithium-sulphur batteries - Binder free carbon nanotubes electrode examined with various electrolytes. *Journal of Power Sources* 2012, 213, 239–248.
14. Zhou, G. *et al.* Fibrous hybrid of graphene and sulfur nanocrystals for high-performance lithium-sulfur batteries. *ACS Nano* 2013, 7, 5367–5375.
15. Huang, J. Q. *et al.* Entrapment of sulfur in hierarchical porous graphene for lithium-sulfur batteries with high rate performance from -40 to 60°C. *Nano Energy* 2013, 2, 314–321.
16. Wang, H. *et al.* Graphene-wrapped sulfur particles as a rechargeable lithium-sulfur battery cathode material with high capacity and cycling stability. *Nano Letters* 2011, 11, 2644–2647.
17. Ji, L. *et al.* Graphene oxide as a sulfur immobilizer in high performance lithium/sulfur cells. *Journal of the American Chemical Society* 2011, 133, 18522–18525 (2011).
18. Zhao, M. Q., Zhang, Q., Tian, G. L., Huang, J. Q. & Wei, F. Space confinement and rotation stress induced self-organization of double-helix nanostructure: A nanotube twist with a moving catalyst head. *ACS Nano* 2012, 6, 4520–4529 (2012).
19. Li, Y. *et al.* One-step synthesis of nano-S/C@PANI composites for lithium-sulfur batteries with high rate and long lifespan. *Journal of Materials Research and Technology* 2022, 20, 3714–3722 .
20. Yuan, H. *et al.* Conductive and Catalytic Triple-Phase Interfaces Enabling Uniform Nucleation in High-Rate Lithium–Sulfur Batteries. *Advanced Energy Materials* 2019, 9, 1–8.
21. Xie, K. *et al.* Ferroelectric-Enhanced Polysulfide Trapping for Lithium–Sulfur Battery Improvement. *Advanced Materials* 2017, 29,1604724.
22. Katiyar, R. K. *et al.* Role of ferroelectric nanoparticles coated separator in improvement of capacity retention at high current density on sulfur/SWCNT composite cathodes for Li-S batteries. *APL Materials* 2023, 11, 1–5.
23. Castillo, I., Mishra, K. K. & Katiyar, R. S. Phase Transition and Energy Storage Density in Lead-Free Ferroelectric $Ba_{1-x}Sr_xTiO_3$ (x = 0.1, 0.3, and 0.7) Capacitors. *Crystals* 2023, 13, 630.
24. Razak, K. A., Asadov, A., Yoo, J., Haemmerle, E. & Gao, W. Structural and dielectric properties of barium strontium titanate produced by high temperature hydrothermal method. *Journal of Alloys and Compounds* 2008, 449, 19–23.
25. Mudinepalli, V. R., Feng, L., Lin, W. C. & Murty, B. S. Effect of grain size on dielectric and ferroelectric

 doi:10.20944/preprints202408.0648.v1

properties of nanostructured $Ba_{0.8}Sr_{0.2}TiO_3$ ceramics. *Journal of Advanced Ceramics* 2015, 4, 46–53.

26. Tripathi, B., Katiyar, R. K., Morell, G., Dixit, A. & Katiyar, R. S. $BiFeO_3$ coupled polysulfide trapping in C/S composite cathode material for Li-S batteries as large efficiency and high rate performance. *Energies* 2021, 14, 1–9.
27. Zhang, B., Qin, X., Li, G. R. & Gao, X. P. Enhancement of long stability of sulfur cathode by encapsulating sulfur into micropores of carbon spheres. *Energy and Environmental Science* 2010, 3, 1531–1537.
28. Singh, M. K., Jang, H. M., Ryu, S. & Jo, M. H. Polarized Raman scattering of multiferroic BiFeO3 epitaxial films with rhombohedral R3c symmetry. *Applied Physics Letters* 2006, 88, 1–3.
29. Xue, L. *et al.* Ferroelectric polarization accelerates lithium-ion diffusion for dendrite-free and highly-practical lithium-metal batteries. *Nano Energy* 2021, 79,105481.
30. Yim, T. *et al.* Effective Polysulfide Rejection by Dipole-Aligned BaTiO3 Coated Separator in Lithium–Sulfur Batteries. *Advanced Functional Materials* 2016, 26, 7817–7823.
31. Li, G. *et al.* Three-dimensional porous carbon composites containing high sulfur nanoparticle content for high-performance lithium-sulfur batteries. *Nature Communications* 2016, 7, 1–10.
32. Deng, C., Wang, Z., Wang, S. & Yu, J. Inhibition of polysulfide diffusion in lithium-sulfur batteries: Mechanism and improvement strategies. *Journal of Materials Chemistry* 2019, A7, 12381–12413.
33. Zhao, M., Li, B. Q., Chen, X., Xie, J., Yuan, H. & Huang, J. Q. Redox Comediation with Organopolysulfides in Working Lithium-Sulfur Batteries. *Chem* 2020, 6, 3297–3311.
34. Das, S. R., Choudhary, R. N. P., Bhattacharya, P., Katiyar, R. S., Dutta, P., Manivannan, A. & Seehra, M. S. Structural and multiferroic properties of La-modified $BiFeO_3$ ceramics. *Journal of Applied Physics* 2007, 101, 3–10.
35. Ding, W., Lu, J., Tang, X., Kou, L. & Liu, L. Ferroelectric Materials and Their Applications in Activation of Small Molecules. *ACS Omega* 2023, 8, 6164–6174.